

The structure of the accretion disk rim in supersoft X-ray sources

E. Meyer-Hofmeister*, S. Schandl, and F. Meyer

Max-Planck-Institut für Astrophysik, Karl Schwarzschildstr. 1, D-85740 Garching, Germany

Received 16 August 1996 / Accepted 2 October 1996

Abstract. Supersoft X-ray sources are characterized by the radiation of a white dwarf with a temperature of some 10^5 K. The compact star is surrounded by an irradiated accretion disk which provides the high optical luminosity. For CAL 87 (Schandl et al. 1996a, 1996b) it could be shown, that this disk has an elevated rim at the outer edge. The impact of the accretion stream from the companion on the disk is important for the rim structure.

More optical observations have recently become available for supersoft sources. Detailed features became known, as short-time variations of the shape of the orbital light curve of RX J0019 (Will & Barwig 1996), the long-term variations of RX J0019 (Greiner & Wenzel 1995) and the changes of RX J0513 between a high and a low state (Alcock et al. 1996). We use our simulation of the orbital light curves (developed for CAL 87) to analyse the disk rim structure of these two other sources in comparison with the observations. We find that a high rim gives good agreement and allows to explain the observations. For the modelling of the high state of RX J0513 the irradiation of disk and secondary by an extended white dwarf is included. The consistent appearance of a high rim feature raises interesting dynamical problems for the stream disk interaction.

Key words: accretion disks – binaries: eclipsing – stars: CAL 87, RX J0019.8, RX J0513.9 – X-rays: stars

1. Introduction

The structure of accretion disks in supersoft X-ray sources (SSS) is strongly affected by the high accretion rate, on order of $10^{-7} M_{\odot}/\text{yr}$, and the irradiation by the central hot white dwarf. It is now commonly accepted, that binary SSS can be understood as white dwarfs accreting matter from a companion star at a rate high enough to produce steady nuclear burning (van den Heuvel et al. 1992). Such a high rate causes a disk structure different from that in low mass X-ray binaries (LMXRBS). SSS differ from classical cataclysmic variables in the white dwarf temperature, which is about 10^5K . The luminosity of the disk originates from reprocessed radiation of the central star. Recently more

data have become available for the source RX J0019.8+2156, hereafter called RX J0019 (Will and Barwig 1996) and, especially from the MACHO Project, for RX J0513.9-6951, hereafter called RX J0513 (Alcock et al. 1996) which allow further insight (for the present status of investigations on SSS see Greiner (1996)). A common feature of all SSS is, that the impact of the accretion stream on the disk presumably leads to a high disk rim. This rim, irradiated by the central white dwarf, acts like a large screen. The reprocessed radiation originating from this extended area becomes the dominant source of optical light. The inner disk and the irradiated secondary star contribute less.

The high optical luminosity of supersoft sources was already earlier attributed to the accretion disk. But only orbital light curves for higher inclination systems with eclipses of white dwarf, disk and secondary star reveal the location where the radiation originates. The detailed orbital light curve of the eclipsing source CAL 87 is the best example. Optical light, UV radiation and X-rays give constraints for the theoretical modelling of the system. In a recent investigation (Schandl et al. 1996a, 1996b) we found from the comparison with the observations that the disk rim is probably vertically high and radially extended over a large range of azimuth. It is the aim of the present paper to clarify whether all supersoft X-ray binaries have disks with a high rim. We want to prove this suspicion for all sources with sufficient observations.

We proceed in the following way. In Sect. 2 we describe the structure of the disk in SSS. Since high bulges were already discussed in connection with LMXRBs we compare the SSS with the LMXRBs. Using the method developed for CAL 87 we model the orbital light curves of other systems to check whether a high disk rim is needed to fit the observations. In Sect. 3 we present a new fit to the light curve of CAL 87, based on the recently derived smaller distance of the LMC. In Sect. 4 we analyse the source RX J0019. We argue, that the short-time changes in the shape of the light curve can be understood by a variation in the shape of the rim. In addition we show, that a systematic change of the rim height due to a general decrease of the mass accretion rate can result in long-term systematic changes of the optical luminosity, as observed. In Sect. 5 we discuss the observations of RX J0513, which show high and low states. We assume, that the low state is comparable to what we see in most SSS, an irradiated disk around a hot white dwarf.

* email: emm@mpa-garching.mpg.de

Table 1. The System Parameters used for the simulations

	P [hr]	d [kpc]	L_{bol} [$10^{37} \frac{\text{erg}}{\text{sec}}$]	\dot{M} [$10^{-7} \frac{M_{\odot}}{\text{yr}}$]	M_{wd} [M_{\odot}]	M_2 [M_{\odot}]	T_2 [K]	i [$^{\circ}$]
RX J0019.8+2156	15.85 ¹	2.1 ¹	0.4 ¹	0.8	0.75	1.5	7 000	56
CAL 87	10.6 ²	47.3 ³	2.2	0.8	0.75	1.5	8 000	78
RX J0513.9-6951	18.24 ⁴	47.3 ³	10.0 ⁵	3.0	1.0	2.0	9 000	15

References: 1 Beuermann et al. (1995), 2 Callanan et al. (1989), 3 Gould (1995), 4 Crampton et al. (1996), 5 Schaeidt et al. (1993)

We model this state in the same way as CAL 87. For the high state we include an extended white dwarf photosphere and the resulting change of irradiation of disk and secondary star. Reinsch et al. (1996a) have shown that the difference in brightness between high and low state can be explained by changes of the photospheric radius. We also include the radius variations in our model. The results indicate, that also this source is consistent with a high disk rim. In Sect. 6 we discuss the relation between mass overflow rate and disk rim height assuming a stochastic velocity distribution of blobs which are produced by the impact of the accretion stream on the disk. In Sect. 7 we summarize the indications for high disk rims in SSS.

2. The structure of the accretion disk

2.1. The bulge of the accretion disk in LMXRBs

Milgrom (1978) had suggested that accretion disks in LMXRBs were geometrically thick. The light curve of the high inclination system 4U 1822-371 observed with HEAO 1 showing a partial X-ray eclipse preceded by a broad minimum proved this assumption. The eclipse was interpreted as being due to the partial occultation of the extended accretion disk corona by the companion. The underlying sinusoidal modulation was interpreted as the obscuration of the corona by the outer accretion disk. This was a first hint to a high disk rim. White and Holt (1982) modelled this orbital X-ray light curve. The best fit included two bulges on the disk rim, one at the point where the disk intercepts the gas stream from the companion star and a second smaller bulge on the opposite side. The height of the rim derived was 0.15 to 0.30 R_{\odot} for disk radii of 0.6 to 0.7 R_{\odot} (depending on the assumed inclination). This was confirmed by work of Mason and Cordova (1982) who showed, using the proposed rim profile, that also the ultraviolet, optical and infrared light curves could be fitted.

Orbital X-ray light curves of several other LMXRBs were later investigated. For a recent review see White et al. (1995). It became clear, that these bulges can be quite extended in azimuth. The dips in the light curves, interpreted as connected with the thickened region, confirm this. White et al. (1995) give examples for the occurrence of dips over about half the orbital cycle (X0748-676) and for essential changes of the depth and the duration from cycle to cycle (X1755-338, X1254-690, X1626-673). The source X1626-673 shows the interesting feature, that the low-level sideband period of the pulsar is probably the result of reprocessing of X-rays on the bulge of the accretion disk

(and/or the companion star). Parmar et al. (1986) mentioned that 'secondary dips' were observed in several systems requiring the presence of a second thickened region at the disk about 180 degree upstream. These dips point to a clumpy structure of the bulge. Schandl (1996) found that the complex dip structure in the X-ray signal of Her X-1 originates from the interaction between accretion stream and the disk, which is tilted and twisted in this system. The features found for the disks in LMXRBs, irradiated by the neutron star, with a moderate accretion rate, are relevant also for disks in close binary SSS, irradiated by the hot steady-burning white dwarf with a mass accretion rate of least a factor of ten higher. Because of the nearly opposite mass ratio in SSS (the secondary is more massive) the phase of the location where the stream hits the disk is slightly different from that in LMXRBs, which influences the rim profile. The fact, that in LMXRBs hard X-rays and in SSS soft X-rays are reprocessed, may result in different albedos (for LMXRBs see de Jong et al. 1996). The optical emission of LMXRBs is dominated by reprocessing of X-rays and it is therefore uncertain to estimate the accretion rate from the visual magnitude. From evolutionary considerations (Bhattacharya 1995) an average mass accretion rate below $10^{-8} M_{\odot}/\text{yr}$ seems adequate. If we assume, that the height of the disk rim is mainly affected by the stream impact, the higher accretion rate in SSS lets us expect that the features found for LMXRBs, a high disk rim and short time variability, are even more pronounced.

2.2. The modelling of the disk in SSS

Luminous X-ray binary sources with very soft spectra had already been detected with the EINSTEIN observatory (Long et al. 1981). CAL 83 and CAL 87 had at this time been classified as LMXRBs and the light curve of CAL 87 was modelled according to this (Callanan and Charles 1989). After the many detections by ROSAT the SSS were established as a new class of objects where the bulk of the X-ray spectrum lies below 0.5 keV. For a review see Hasinger (1994). It is now commonly accepted, that the close binary SSS are systems where a Roche lobe filling secondary star transfers mass at a high rate to a steady-burning white dwarf via an accretion disk (van den Heuvel et al. 1992). The companion star has about double the mass of the white dwarf (a mass ratio inverse to that of LMXRBs). A computer code for modelling light curves of SSS was recently developed by Schandl et al. (1996a, 1996b) and used to fit the light curve of CAL 87.

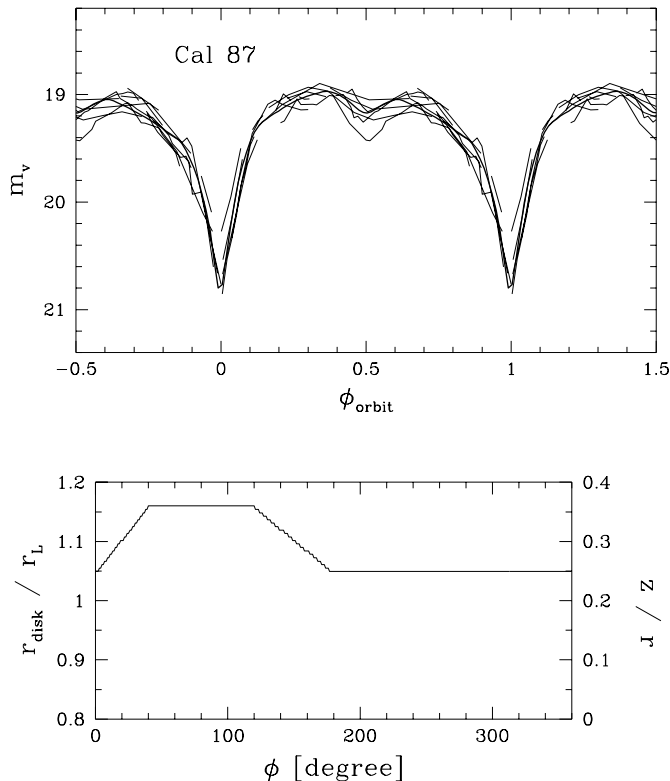


Fig. 1. The light lines in the upper diagram show the composite V light curve of CAL 87. The photometry is done between November 1985 and December 1992 (Schmidtke et al. 1993). We connect data points observed during one cycle to stress that the variability of the data is larger from cycle to cycle than during one cycle. The heavy line shows our fit to these data. The main difference of the parameters used here (Table 1) and in Schandl et al. (1996a, 1996b) is the smaller distance to the LMC and a different shape of the spray at the rim shown in the lower diagram.

Our method takes into account (1) the height of the accretion disk consistent with its irradiation, (2) an accretion disk rim, which is irradiated where facing the white dwarf and (3) a Roche lobe filling (non-spherical) irradiated secondary star, shaded by the disk rim. Vertical structure computations were carried out to evaluate the height of the inner disk, which depends on the irradiation and vice versa. The orbital period and the distance are known. We choose the following parameters for calculating the light curve (see table 1): the mass of white dwarf and secondary star and the accretion rate (based on the van den Heuvel model). We further assume the temperature of the secondary's non-irradiated backside according to its mass and the chemical composition (Schaerer et al. 1993, Schaller et al. 1992). As found from the work for CAL 87 energy transfer from the irradiated to the non-irradiated part of the surface seems necessary (the angular width of the spreading being 45°). The efficiency of the radiation reprocessing we take as 0.5. After we have chosen the stellar masses and the accretion rate and with the known orbital period, the bolometric luminosity of the white dwarf and the separation of the stars follow and with this

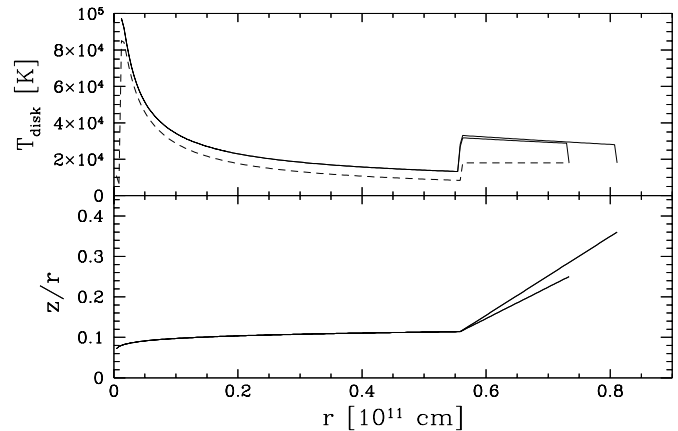


Fig. 2. CAL 87, disk surface temperature and z/r as a function of radius for the inner part and the bulge (upper and lower line for the higher and lower parts of the rim profile in Fig. 1). Dashed line disk temperature without irradiation. Rim temperature on the outer, non-illuminated side 18 000 K.

the disk size (80% of the Roche lobe according to the models of Paczyński (1977) and Papaloizou & Pringle (1977)). The distance is known for the LMC sources (Gould 1995) and roughly for the galactic source (Beuermann et al. 1995). The inclination can be judged from the comparison with the observed light curve of the individual source. A detailed description is given in Schandl et al. (1996a, 1996b).

3. The source CAL 87

Corresponding to the new value for the distance to the LMC derived by Gould (1995) we repeat the modelling of Cal 87 published recently in Schandl et al. (1996a, 1996b). We also take now into account that the inner part of the accretion disk reaches down to the surface of the white dwarf. As a result, the lower hemisphere of the white dwarf cannot illuminate the upper disk surface.

We model the shape of the disk rim as a bulge between 0° and 180° following the stream impact (Fig. 1) and a remaining part of constant height. In our calculations of the free fall trajectories we have found that most of the sprayed matter falls back to the accretion disk surface after travelling half way around. The remaining spray matter will form a high rim of blobs moving vertically up and down outside of the original disk, surrounding it with Keplerian velocity. This is simulated by the shape of the bulge. Fig. 2 shows the resulting disk surface temperature. This temperature, especially its increase in the rim area is derived consistent with the irradiation from the hot white dwarf. Fig. 3 shows the temperatures on the companion star. We used the smoothed distribution in the modelling as mentioned earlier.

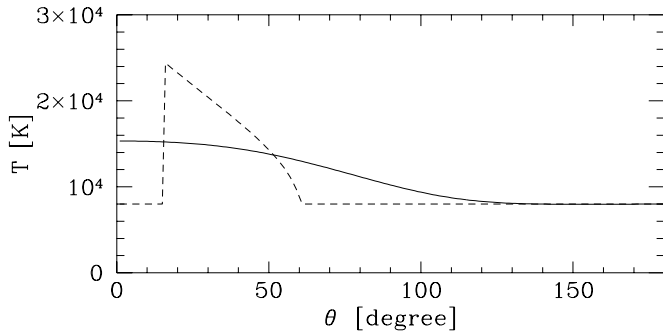


Fig. 3. CAL 87, surface temperature of the companion from the inner Lagrangian point ($\theta = 0$) to a pole ($\theta = 90$) and further to the backside of the disk. The dashed line includes irradiation and shading by the disk, the solid line shows the temperature distribution smoothed by energy transfer along the surface. Temperature of non-illuminated side 8 000 K.

4. The source RX J0019.8+2156

4.1. The orbital light curve

RX J0019 was discovered during the ROSAT All-Sky-Survey. It was the first supersoft source found in our galaxy (Reinsch et al. 1993). Beuermann et al. (1995) obtained optical photometric and spectroscopic data as well as UV and X-ray spectra. The fact that this galactic source is about 7 magnitudes brighter than the SSS in the Magellanic Clouds allows observations with a smaller telescope. Will and Barwig (1996) observed it using the high speed multi-channel-photometer MCCP (Barwig et al. 1987) at the 80 cm Wendelstein Observatory during 25 nights from 1992 to 1995.

The observed blue flux of Will & Barwig (Fig. 4, in their paper Fig. 3) is given in relative intensities. From the comparison of data from Beuermann et al. (1995) and Will & Barwig (1996) one finds that 0.5 in the arbitrary units for the intensity corresponds to a blue flux of 12.76 magnitudes. Accordingly we choose the luminosity ($4 \cdot 10^{36}$ erg/sec) and the distance (2.1 kpc). Both values are within the range given by Beuermann et al. (1995).

Following the model of Meyer & Meyer-Hofmeister (1996) RX J0019 might now not be in the state of steady hydrogen burning (compare Sect. 4.3). This affects the derivation of white dwarf masses from the model of van den Heuvel (1992). We assume stellar masses and an accretion rate comparable to CAL 87. The secondary's temperature is assumed to be 7 000 K.

Our simulation allows to determine the inclination of the system from the depth of the primary minimum at orbital phase 0 (see Fig. 5). We find 56° as best value and use this in all following simulations.

4.2. Short-time changes of the shape of the orbital light curve

The orbital period of RX J0019, 15.85 hr, makes it difficult to observe the optical light curve over the full cycle. Despite this it became clear, that the shape of the light curve varies from

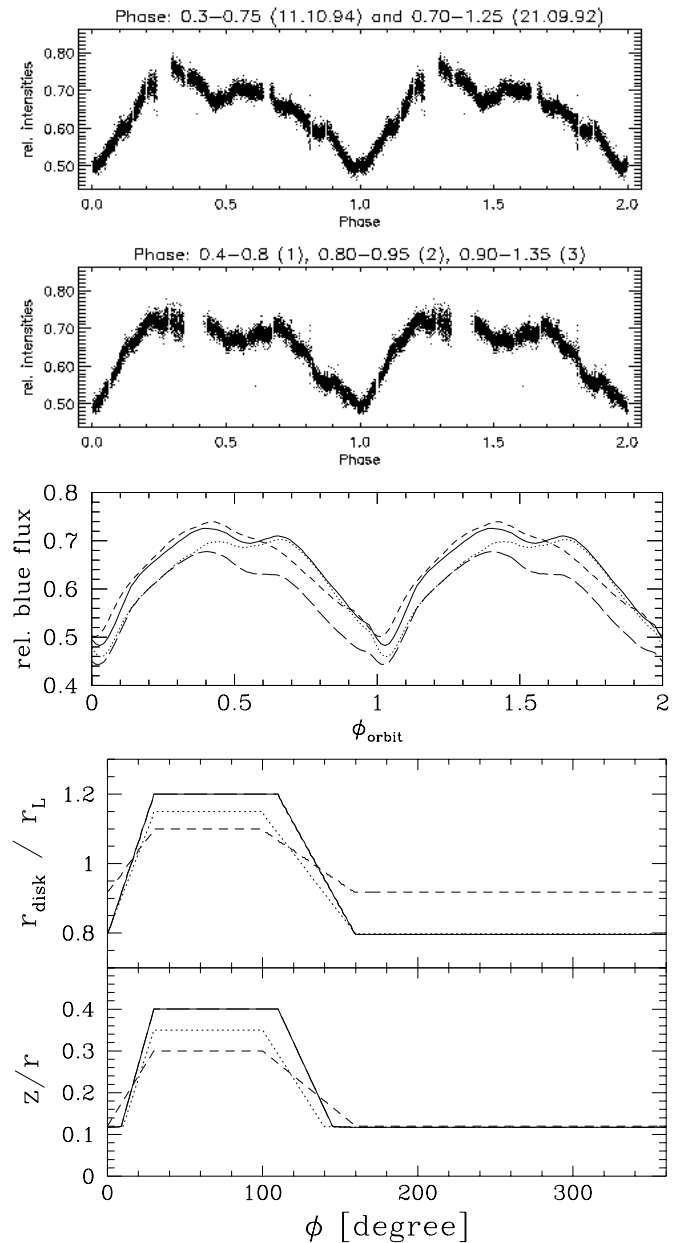


Fig. 4. Simulation of the light curve of RX J0019 with different rim profiles. Upper two panels: mean blue flux of RX J0019 observed between 9/1992 and 10/1995 at the Wendelstein observatory (from Will & Barwig 1996); third panel: results of our simulation for different shapes and temperatures of the disk rim. Corresponding radii and values of z/r in the lower two diagrams (same type of line). The spray temperature is 18 000 K (solid and short-dashed lines) or 20 000 K (dotted line) or 16 000 K (long dashes, same profile as solid line).

night to night (Will and Barwig 1996). We argue, that this can be caused by fluctuations in the rate of mass overflow from the companion star, resulting in changes of the disk rim profile. We discuss later (Sect. 6) how the blobs produced by the stream impact form a disk rim of a height depending on the accretion rate. Different from CAL 87 there is no complete light curve which we can try to reproduce. We therefore calculate light curves in order to reproduce different features of the observed data. Fig. 4

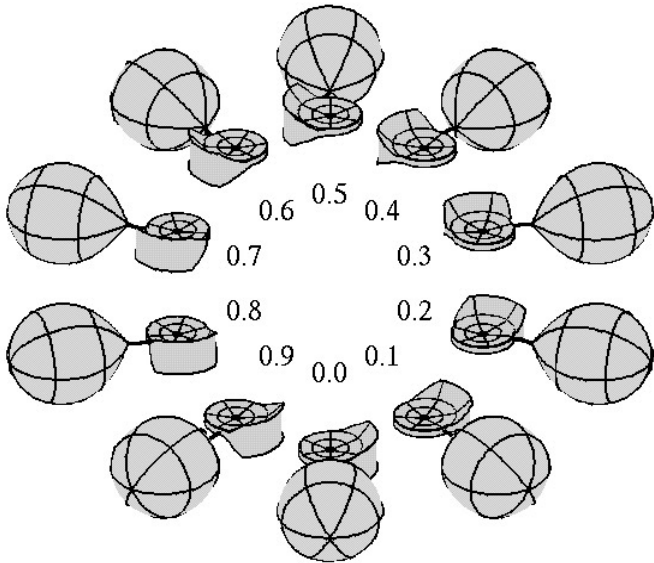


Fig. 5. Varying aspect of disk and secondary star of RX J0019 during the orbit (example solid line in Fig. 4)

shows different light curves with chosen disk extension and rim height. In Fig. 6 the contributions of disk and star are given separately. The aspect of the system displayed in Fig. 5 illustrates the geometry. We consider now variations of the light curve at different orbital phases.

4.2.1. The light curve near the secondary minimum

At different observing runs the flux is found not to be the same at orbital phase 0.5, as shown in Fig. 4. We conclude that the varying depth and width of the minimum is caused by changes in the shape of the rim.

From our calculations we find, that the flux between orbital phase 0 and 0.5 is dominated by the illuminated inner side of the high rim bulge (see Fig. 5). At later phases the cooler but larger outer area of the non-illuminated edge of the rim yields most of the optical light. The transition occurs at orbital phase 0.5. The shape of the rim is therefore very important at this phase.

4.2.2. The light curve at phases of high brightness

The brightness before and after phase 0.5 depends also on the shape and temperature of the bulge. The solid curve in Fig. 4 has nearly the same maximal flux prior and after phase 0.5. For the same spray temperature, but a changed rim profile, we find a lower luminosity after phase 0.5 (short-dashed line). The variation between these two solutions appears very similar to the difference in the observations in the first two panels in Fig. 4. Reducing only the temperature of the non-illuminated spray yields a lower luminosity especially after phase 0.5 (long-dashes). Otherwise we obtain the same luminosity at these later phases for a smaller bulge and a slightly higher temperature (dotted line), but a reduced luminosity before phase 0.5.

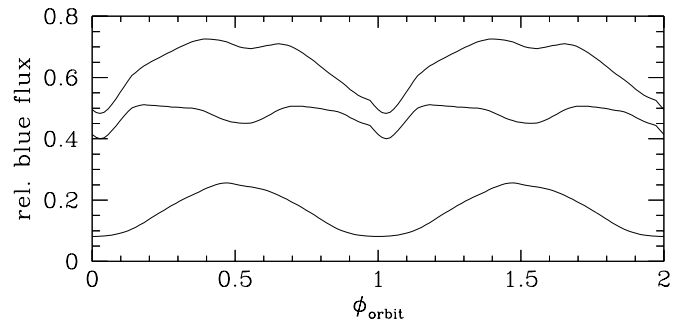


Fig. 6. Contributions to the light curve (upper line total flux, example solid line in Fig. 4) from companion star (lowest line) and accretion disk with high rim (middle line).

4.2.3. The light curve near the primary minimum

The luminosity around primary minimum also varies with the shape of the rim. In the observations it varies between 0.45 and 0.5 in relative intensities (Will & Barwig 1996).

In the observed light curves in Fig. 4 we see small 'steps' around orbital phases 0.9 and 0.1. They are real and not generated by joining data from different observing runs together. From our simulations (see Fig. 6) we find an explanation for this feature in the eclipse ingress and egress of the accretion disk.

Variation of the rim shape can also affect the orbital phase of the primary minimum because the location of the minimum varies around phase 0. This might explain the deviations of the observed from the calculated minimum of up to 0.01 in orbital phase (Will & Barwig 1996).

4.3. Long-term variations of the optical brightness

An impressive piece of information on SSS is the optical light curve of RX J0019 over hundred years derived from photographic plates at Harvard and Sonneberg observatory (Greiner and Wenzel 1995). After 1930 so many observations were available, that many brightness values in the light curve of Greiner and Wenzel (Fig. 2) contain 9 or more individual measurements. Fluctuations arising from the fact, that the measurements belong to different orbital phases are then small and it is possible to study the long-term evolution. Three states can be recognized. After a decrease from peak luminosity (as in the years around 1935 and 1970) the source is observed at about constant brightness for one decade. Finally the brightness drops to a level about 0.5 magnitude lower.

We interpret this as a long lasting cooling after a short phase of nuclear burning, and finally a decreasing mass transfer from the companion star (Meyer and Meyer-Hofmeister 1996). It is interesting, that the changes of X-ray flux are very small, from 2.1 cts/s in 1990 to 2.0 cts/s in 1992 and 1993 (Beuermann et al. 1995) while the visual luminosity has varied by 0.5 magnitude. This lets us argue, that, if the white dwarf temperature does not change much, the variations can only be caused by a change of the shape of the reprocessing area, i.e. the disk bulge. If the height of the disk rim essentially depends on the mass accretion

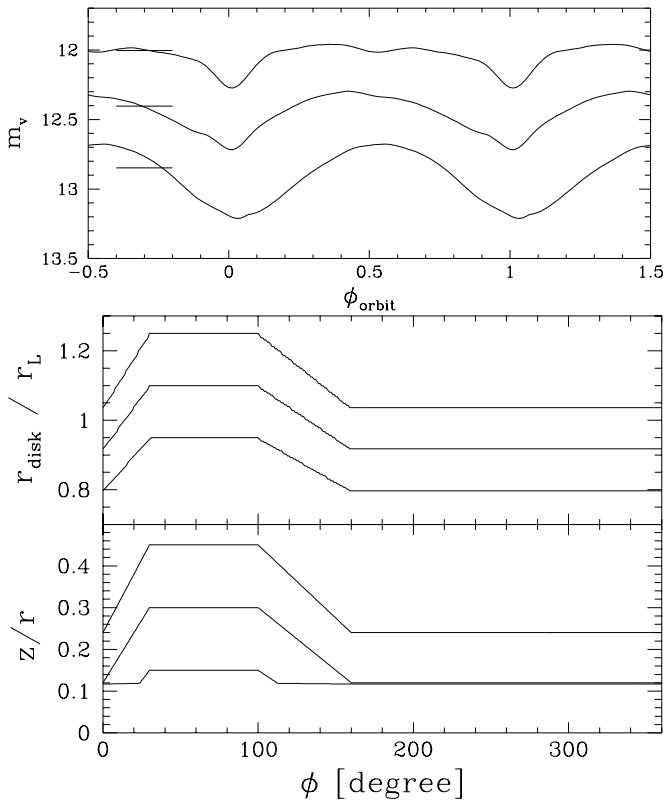


Fig. 7. Visual light curve of RX J0513.9-6951, simulations for long-term changes of the rim height. Proportional changes of values z/r and radial extension of the spray region surrounding the accretion disk rim. The solution from Fig. 6 (there in the blue filter) is the middle line in each panel. Vertical dashes show the mean visual magnitudes averaged over the orbital phase interval 0.1 to 0.9 (see text).

rate it is plausible, that the luminosity can become lower during a late phase of cooling due to a lower mass overflow rate, when also the irradiation of the companion star by the hot white dwarf is less important.

To evaluate how much the brightness changes with disk rim height in our modelling we assumed as a simple case a proportional variation in z/r and the radial extent of the disk. The light curves and especially the differences in the simulated average brightness are shown in Fig. 7 (horizontal dashes). For the latter, values of phases 0.9-0.1 were left out (these are the low values near eclipse) corresponding to the determination of averages in Greiner and Wenzel (1995). We see that a change in the rim height easily explains a decrease by 0.5 magnitude as observed. The recent luminosity increase (X-ray flux still unchanged), would, within the framework of our considerations, be interpreted as a now again higher rim and a higher mass transfer rate. A more detailed description of the observations and their modelling will be presented in a separate investigation (Barwig et al., in prep.).

5. The source RX J0513.9-6951

5.1. Observations

After the ROSAT observations had led to the discovery of several SSS an intense search for the optical/UV counterparts of these objects started. More detailed information for these systems became available. RX J0513 was observed with different telescopes. Recent results are described in work of Cowley (1995), Crampton et al. (1996), Motch & Pakull (1996) and Reinsch et al. (1996b). Exceptional information could be collected using the monitoring capabilities of the MACHO project. These continuous optical observations show the history for 3 years with a high state from which the brightness drops by about 1 magnitude every 100 to 200 days to the shorter lived low state (Alcock et al. 1996). In a detailed investigation on the nature of this SSS (Southwell et al. 1996) it is shown, that the available X-ray observations (on- and off-states, Schaeidt et al. 1993, Schaeidt 1996) are consistent with the assumption that X-rays are detected only during the low state and it was suggested, that the low states are phases where the white dwarf radius is small during nuclear shell burning. The smaller white dwarf then (for constant luminosity) has a higher temperature at the photosphere and is detectable for ROSAT. Concerning the high state Pakull et al. (1993) had suggested earlier that the white dwarf radius might change in direct response on the accretion rate. This was based on calculations of Kato (1985). Reinsch et al. (1996a) have shown that a brightness difference between high and low state can be explained by changes of the photospheric radius and the resulting different irradiation, based on a Roche lobe filling flat disk.

5.2. The modelling of the low state

In the following we describe the procedure of our modelling. During the low state RX J0513 seems comparable to other SSS as CAL 83 or CAL 87. We determined a light curve assuming the rim profile and spray temperatures as for CAL 87 (compare Fig. 1). The system parameters used are listed in table 1. We take the same masses as Reinsch et al. (1996a). From the model of van den Heuvel et al. (1992) we deduce a bolometric luminosity of 10^{38} erg/sec. The chosen inclination (15°) leads to an orbital modulation of 0.065 magnitudes similar to that in the optical observations of Motch & Pakull (1996) of the source in the high state. From their work we also take the mean visual brightness of 16.6 for our comparison with the observations. Slightly different mean values can be found from different investigations of RX J0513. Also different filters were used. The source might be brighter. Theoretically higher masses for the white dwarf and the secondary star would be connected with a larger disk. This, and a higher mass accretion rate (according to the van den Heuvel model) would yield a higher luminosity. This might be indicated by the timescales of the relevant phases described in work of Kato (1996) which points to high white dwarf masses.

For the low state we take the white dwarf radius 10^9 cm. The resulting orbital light curve is the lowest line in Fig. 8. We show this curve together with the photometric data of the

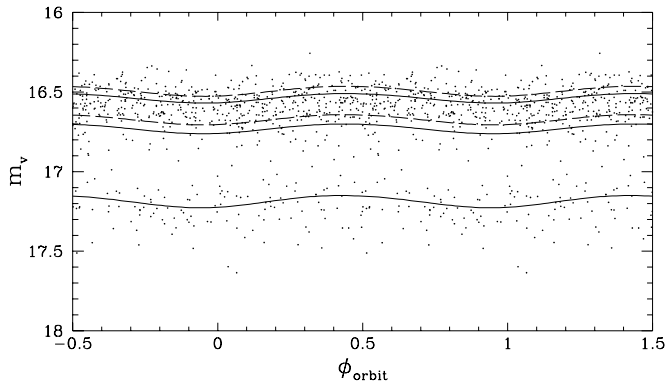


Fig. 8. Photometric data of RX J0513 of Alcock et al. (1996) folded over the orbital period. $\Delta m=0$ in this diagram corresponds to 16.6 magnitude (Motch and Pakull 1996). The values are concentrated around low and high state. Solutions for white dwarf radii of 10^9 cm, $3 \cdot 10^{10}$ cm and $6 \cdot 10^{10}$ cm with reprocessing efficiency $\eta = 0.5$ are drawn with solid lines. The dashed lines correspond to $\eta = 0.6$ for the same high state radii.

MACHO light curve ordered according to the ephemeris $T_0 = \text{JD } 2448857.832 + 0.76278 E$ (Alcock et al. 1996). Low and high states can be recognized. The low state with the small radius corresponds to the state of CAL 87 and RX J0019 and the level of the total optical luminosity in our simulation is reproduced well. The scatter in the observations of about 0.3 magnitude in the long-term light curve of RX J0513 (Alcock et al. 1996) leads to a scatter also in the orbital light curve. It is comparable to that found for CAL 87.

5.3. The modelling of the high state

For the modelling of the high state we include an extended white dwarf atmosphere and therefore an extended light source illuminating the surrounding disk and the secondary. For the illumination of the disk we integrate the luminosity from a sphere, the size equal to the white dwarf radius. We integrate over that part of the sphere which is visible from the disk surface. For the illumination of the secondary we use a more simple description because its contribution is smaller. We calculate the illumination as from two point sources each of half the total luminosity above and below the disk center at equivalent height $R_{\text{wd}}^{\text{eff}} = \frac{4}{3\pi} R_{\text{wd}}$. In Fig. 8 we show together with the low state solution the high state solutions for radii $3 \cdot 10^{10}$ cm and $6 \cdot 10^{10}$ cm. We computed high state solutions with two values for the reprocessing efficiency $\eta = 0.5$ and $\eta = 0.6$ (solid and dashed lines in Fig. 8). We want to emphasize that the cross section for photoionization strongly depends on the frequency of the irradiated photons. Therefore, we expect that the lower white dwarf temperature in the high state allows a more effective reprocessing. The higher value of η results in a luminosity about 0.05 magnitude higher. Fig. 9 shows the temperatures of disk and secondary.

It is interesting to see how the luminosity of the system increases with the white dwarf radius. Our detailed simulations are in good agreement with the observations and confirm the

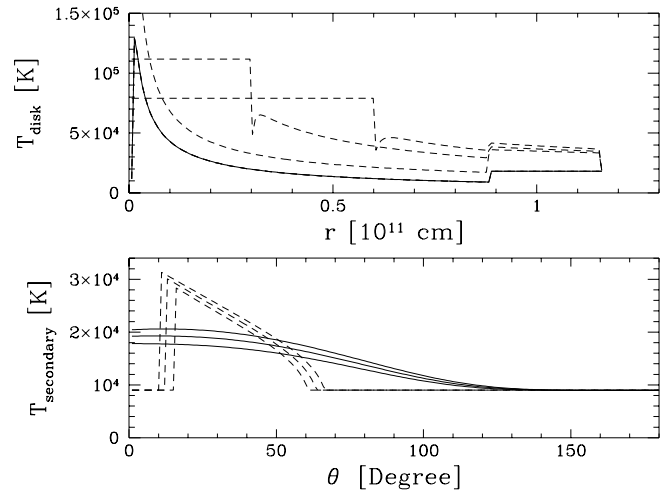


Fig. 9. The temperatures of disk and secondary for the simulations in Fig. 8 with $\eta = 0.5$. Solid line temperature of non-illuminated disk. For the high state solutions temperatures of the white dwarf is drawn for the area covered by the extended white dwarf. The small dip at the white dwarf radii is due to numerical effects, without effect on the simulation. The temperature of the secondary is shown in the same way as in Fig. 3.

picture that there is a slow decrease of the white dwarf photospheric radius during the high state until the radius finally drops by about a factor of 30 on entering the low state. The source spectrum then moves to lower energies undetectable by ROSAT.

Reinsch et al. (1996) have performed a first calculation of the optical luminosity of RX J0513 for extended radii of the white dwarf, the same radii as we assumed now. For the brightness in the two states they obtain 17.8 and 16.9 magnitudes with the distance modulus 18.5 (we used the value 18.37 recently derived by Gould (1995)). We find 17.25 and 16.7 magnitudes for white dwarf radii of 10^9 cm and $3 \cdot 10^{10}$ cm, respectively. The difference between both calculations of the low state results mainly from the different description of the accretion disk. We find the main contribution to the optical light in the reprocessed radiation of the high disk rim. Without such a rim Reinsch et al. (1996) find a lower luminosity although their disk extends out to the Roche lobe. For a flat disk the cosine of the angle of incidence of the radiation is very different for the two white dwarf radii. The disk rim in our model is illuminated at finite angles even in the case of a central point source.

We also investigated the effect of the wind from the extended white dwarf photosphere (Kato and Hachisu 1994). The density profile of the wind is proportional to r^{-2} . We simulated the radially decreasing scattered light source by six point sources, three on each side of the disk, at height 1, 2 and $4 R_{\text{wd}}^{\text{eff}}$ from the disk with luminosities weighted 1, $\frac{1}{2}$ and $\frac{1}{4}$, respectively, representing the light centers of consecutive shells of wind. The total luminosity is unchanged. This more detailed wind model compared to a solution including only two point sources (sim-

ulating no wind) yields an enhancement of visual luminosity of 0.05 magnitudes.

6. Relation between mass overflow rate and disk rim height

We discuss now the consequences of the accretion stream impact on the disk rim. Underneath the impact area a dense layer arises in which shocked impact and disk gas stream along each other with a high shear. The high density of the shocked layer results from the ram pressure of the impact together with the efficient cooling by radiative transport outward through the impact area. On moving out from underneath the impact area pressure release and ensuing instabilities will probably transform this layer material into a stochastic ensemble of clumps or blobs of various velocities and sizes. The mean stochastic velocity is related to the shear velocity and this allows to estimate the mean height to which such an ensemble of blobs rises above the disk surface. The height *distribution* will then be an exponential decrease of blob number density with height. The absolute value of the blob number density is that which transports the mass accretion rate as the blob ensemble moves around the disk.

Where does such a screen of gas clumps become opaque? To answer this, one has to know the covering cross section of the blobs. Above the disk, the cool blob gas will expand to equilibrium pressure with the surrounding coronal gas. The latter may be estimated from the irradiating flux. The blob temperature is also irradiation determined. It turns out that the blobs are optically thick for the situation typical for SSS.

Since the original density and characteristic scale of stochastic 'turbulent' elements are those of the shear layer, one has the final blob size as the original length scale expanded according to the density expansion. This yields the characteristic cross section of the blobs and together with their height distribution the covering factor as function of height. The apparent disk height is then that at which this covering factor is about 1. Since the dependence on the mass accretion rate \dot{M} can be traced through this analysis it is possible to determine the functional relation between apparent disk height and mass accretion rate. We show this relation in Fig. 10. The resulting estimated numerical values are in reasonable agreement with disk heights as indicated from light curve modelling in this paper.

A more detailed analysis of the discussed problem will be given separately (Meyer, in prep.).

7. Conclusions

After the discovery of SSS in X-rays optical photometric and spectroscopic observations have been performed for several of them. For binaries with known orbital period the phase dependent light curve can then be modelled. The radiation from the disk is important (Meyer and Meyer-Hofmeister 1995, Popham and DiStefano 1996). This offers the possibility to gain detailed structure information from modelling orbital light curves. Based on data for CAL 87, RX J0019 and RX J0513 we find the following features.

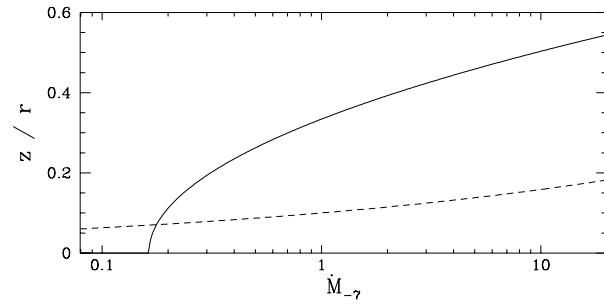


Fig. 10. Height of the opaque screen of blobs at the Disk rim as function of mass accretion rate in units of disk radius r and $10^{-7}M_{\odot}/y$ (solid line) and height of the optically thick standard disk (dashed line).

(1) The height of the bulge is up to $z/r = 0.4$ at its maximum. This is in agreement with the SPH simulations of the stream-disk impact by Armitage and Livio (1996).

(2) Moderate changes of the rim profile explain short-time variations of the shape of the orbital light curve (CAL 87 and RX J0019).

(3) A lower rim height probably caused by a systematically lower mass overflow rate leads to a brightness decrease of order 0.5 magnitude (RX J0019).

(4) Modelling the high and low state of RX J0513 with a high disk rim is able to reproduce the observed brightness of both states, the difference being caused by a large photospheric radius in the high state. A slight dependence of the albedo on the white dwarf temperature is indicated.

These findings suggest the picture that blobs, produced by the stream impact, bounce up and down at the disk rim. Up to a certain vertical height the 'curtain' of blobs appears optically thick and acts as a large screen for the radiation from the white dwarf. Above this vertical height the blobs allow the radiation to pass through. If such a blob crosses the line of sight to the observer, it absorbs radiation. In LMXRBs X-ray dips confirm this phenomenon.

The observations for SSS together with the experience from LMXRBs and some indications from cataclysmic variables point to a uniform picture of the rim structure, determined by the mass overflow rate.

Acknowledgements. We thank Paul Schmidtke for unpublished data on CAL 87 and are also grateful to Heinz Barwig and Tobias Will who immediately gave us the observational data on RX J0019. We thank Karin Southwell for kindly providing the original observational data on RX J0513 for our simulations.

References

- Alcock C., Allsman R.A., Alves D. et al., 1996, MNRAS, in press
- Armitage P.J., Livio M., 1996, Space Telescope Science Institute Preprint Series No. 1062
- Barwig H., Schandl S., Will T., 1996 (in preparation)
- Barwig H., Schoembs R., Buckenmayer C., 1987, A&A 175, 327
- Beuermann K., Reinsch K., Barwig H. et al., 1995, A&A 294, L1

- Bhattacharya D., 1995, X-ray binaries, eds. W.H.G. Lewin, J. van Paradijs, E.P.J. van den Heuvel, Cambridge Astrophysics Series, p. 233
- Callanan P.J., Charles P.A., 1989, ESA SP-296, 23rd ESLAB Symposium, p. 139
- Cowley A., 1995, IAU Symp. 165, Compact Stars in Binaries, eds. E. van den Heuvel, J. van Paradijs, Kluwer, in press
- Crampton D., Hutchings J.B., Cowley A.P. et al., 1996, ApJ 456, 320
- de Jong J.A., van Paradijs J., Augusteijn T., 1996, submitted to A&A
- Gould A., 1995, ApJ 452, 189
- Greiner J., 1996, Workshop on Supersoft X-ray Sources, Garching, 1996, ed. J. Greiner, Lecture Notes in Physics No. 472, Springer Verlag
- Greiner J., Wenzel W., 1995, A&A 294, L5
- Hasinger G., 1994, Reviews in Modern Astronomy 7, ed. G. Klare, Astron. Gesellschaft, p. 129
- Kato M., 1985, PASJ 37, 19
- Kato M., 1996, Workshop on Supersoft X-ray Sources, Garching, 1996, ed. J. Greiner, Lecture Notes in Physics No. 472, Springer Verlag, p. 15
- Kato M., Hachisu I., 1994, ApJ 437, 802
- Long K.S., Helfand D., Grabosky D.A., 1981, ApJ 248, 925
- Mason K.O., Cordova F.A., 1982, ApJ 262, 253
- Meyer F., 1996, to be submitted to A&A
- Meyer F., Meyer-Hofmeister E., 1995, Cataclysmic Variables, eds. A. Bianchini et al., Kluwer Academic Publishers, p. 463
- Meyer F., Meyer-Hofmeister E., 1996, Workshop on Supersoft X-ray Sources, Garching, 1996, ed. J. Greiner, Lecture Notes in Physics No. 472, Springer Verlag, p. 153
- Milgrom M., 1978, AJ 208, 191
- Motch C., Pakull M.W., 1996, Workshop on Supersoft X-ray Sources, Garching, 1996, ed. J. Greiner, Lecture Notes in Physics No. 472, Springer Verlag, p. 127
- Paczyński B., 1977, ApJ 216, 822
- Pakull M.W., Motch C., Bianchi L., 1993, A&A 278, L39
- Papaloizou J., Pringle J.E., 1977, MNRAS 181, 441
- Parmar A.N., White N.E., Giommi P., Gottwald M., 1986, ApJ 308, 199
- Popham R., DiStefano R., 1996, Workshop on Supersoft X-ray Sources, Garching, ed. J. Greiner, Lecture Notes in Physics No. 472, Springer Verlag, p. 65
- Reinsch K., Beuermann K., Thomas H.-C., 1993, Astron. Ges. Abstr. Ser. 9, 41
- Reinsch K., van Teeseling A., Beuermann K., Abbott T.M.C., 1996a, A&A 309, L11
- Reinsch K., van Teeseling A., Beuermann K., Thomas H.-C., 1996b, Workshop on Supersoft X-ray Sources, Garching, ed. J. Greiner, Lecture Notes in Physics No. 472, Springer Verlag, p. 173
- Schaeidt S., 1996, Workshop on Supersoft X-ray Sources, Garching, ed. J. Greiner, Lecture Notes in Physics No. 472, Springer Verlag, p. 159
- Schaeidt S., Hasinger G., Trümper J., 1993, A&A 270, L9
- Schaerer D., Meynet G., Maeder A., Schaller G., 1993, ApJ Suppl 98, 523
- Schaller G., Schaefer D., Meynet G., Maeder A., 1992, A&AS 96, 269
- Schandl S., 1996, A&A 307, 95
- Schandl S., Meyer-Hofmeister E., Meyer F., 1996a, Workshop on Supersoft X-ray Sources, Garching, ed. J. Greiner, Lecture Notes in Physics No. 472, Springer Verlag, in press
- Schandl S., Meyer-Hofmeister E., Meyer F., 1996b, A&A in press (see also 1995, MPI für Astrophysik report no. 912)
- Schmidtke P.C., McGrath T.K., Cowley A.P., Frattare L.M., 1993, PASP 105, 863
- Southwell K.A., Livio M., Charles P.A., O'Donoghue D., Sutherland W.J., 1996, submitted to ApJ
- van den Heuvel E.P.J., Bhattacharya D., Nomoto K., Rappaport S.A., 1992, A&A 262, 97
- White N.E., Holt S.S., 1982, ApJ 257, 318
- White N.E., Nagase F., Parmar A.N., 1995, X-ray binaries, eds. W.H.G. Lewin, J. van Paradijs, E.P.J. van den Heuvel, Cambridge Astrophysics Series, p. 1
- Will T., Barwig H., 1996, Workshop on Supersoft X-ray Sources, Garching, ed. J. Greiner, Lecture Notes in Physics No. 472, Springer Verlag, p. 99